Advanced physics and algorithms in the IBA DataFurnace

N.P. Barradas [a,b,*], C. Jeynes [c]

[a] *Instituto Tecnológico e Nuclear, E.N. 10, Apartado 21, 2658-953 Sacavém, Portugal*
[b] *Centro de Física Nuclear da Universidade de Lisboa, Av. Prof. Gama Pinto 2, 1649-003 Lisboa, Portugal*
[c] *Surrey Ion Beam Centre, University of Surrey, Guildford, Surrey GU2 7XH, England, United Kingdom*

Abstract

The IBA DataFurnace (NDF) is a general purpose program for analysis of IBA data. It currently includes Rutherford backscattering (RBS), elastic (non-Rutherford) backscattering (EBS), elastic recoil detection analysis (ERDA), non-resonant nuclear reaction analysis (NRA), and particle induced X-ray emission (PIXE). Here we discuss recent developments in the advanced physics capabilities implemented in NDF, supported by advanced algorithms. Examples of real life hard cases are given that illustrate the issues discussed.
© 2007 Elsevier B.V. All rights reserved.

1. Introduction

The IBA DataFurnace (NDF) is a general purpose program for analysis of IBA data [1]. It currently includes Rutherford backscattering (RBS), elastic (non-Rutherford) backscattering (EBS), elastic recoil detection analysis (ERDA), non-resonant nuclear reaction analysis (NRA), and particle induced X-ray emission (PIXE).

We discuss recent developments in the advanced physics capabilities implemented in NDF supported by advanced algorithms. The physics implemented includes plural and multiple scattering; accurate simulation of buried resonances; improved simulation of the low energy yield, which is one of the hardest problems in RBS simulation; interface and surface roughness; inclusions, voids and quantum dots; first principles pulse pile-up calculation including three-pulse pile-up.

This is supported by algorithms that allow the user to self-consistently and automatically fit any number of spectra from any combination of the techniques supported, taken from the same sample, with the same depth profile. Incidentally, this makes differential PIXE a simple procedure. The sample components may be expressed as molecules as well as elements, and molecules may have fixed or fitted stoichiometry, thus correlating the signals of different elements. Calculation of errors and confidence limits on all parameters is made by a user-friendly Bayesian inference (BI) algorithm. Furthermore, determination of stopping powers and scattering cross sections from RBS, EBS or ERDA spectra is implemented in NDF using its BI capabilities. Examples of real life hard cases are given that illustrate the issues discussed.

2. Advanced physics

We show in Fig. 1 the RBS spectrum of a $Si/(Ti_{0.4}Al_{0.6}N$ 25.2 Å/Mo 14.9 Å$)_{\times 10}$ multilayer. The experimental conditions have been given in detail elsewhere [2]. We note that the sample was tilted 85° in the Cornell geometry, so the angle with the sample surface is 5° on the way in and 4.7° on the way out. This extreme grazing geometry, together
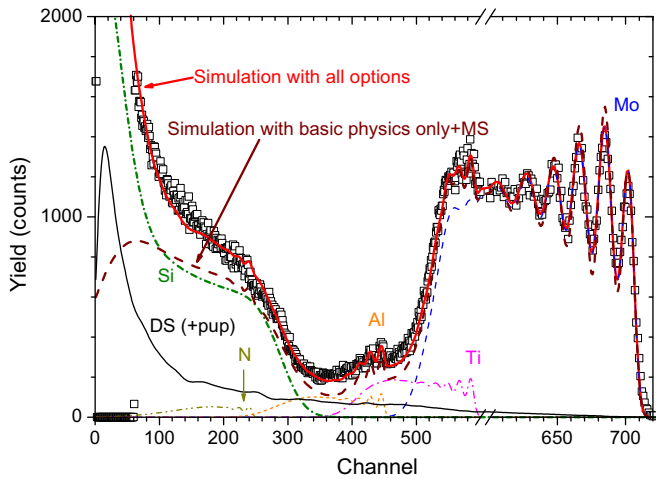
Fig. 1. RBS spectrum of a Si/$(Ti_{0.4}Al_{0.6}N$ 25.2 Å /Mo 14.9 Å$)_{\times 10}$ multilayer measured at 5° grazing angle. A full simulation including double scattering (DS), pulse pile-up (pup), roughness and an improved low energy yield calculation is shown. The calculated partial signals of the elements are shown. A simulation including only basic physics (but with the correct energy straggling) is also shown for comparison.

with a 0.6 nm surface roughness measured with AFM, means this is one of the hardest problems for simulation.

First, the main contribution to energy spread is multiple scattering, which must be included or unrealistic interface mixing will be derived by the data analysis [3]. We used the code DEPTH [4] to calculate the energy spread including all relevant effects. However, at grazing angle the multiple scattering theory that DEPTH implements [5] becomes increasingly inaccurate for larger depths of interaction. Therefore, for the Si substrate signal, we used Bohr straggling scaled by a factor such that at the Si surface the straggling is equal to what is calculated for DEPTH.

Nevertheless, the resulting simulation (also shown in Fig. 1), which includes basic physics plus correct straggling, is still far from the data. The simulated Mo peaks are sharper than the data, because the surface roughness was ignored. Once it is taken into account, using the models given in [6,7], the simulation becomes near perfect in that region. The effect of inclusions and quantum dots is also implemented in NDF [8].

Also, the full simulation included the effect of pulse pile-up [9] calculated with the algorithm of Wielopolski and Gardner [10], which is based on first-principles statistical considerations, and requires as input only know parameters such as the livetime or amplifier characteristics (e.g. shaping time). The contribution of double scattering (DS), i.e. where the beam undergoes two large angle scattering events, is also included [11]. This leads to a dramatic improvement in the quality of the simulation because DS at grazing angles is the largest contribution to the background and already changes the yield at fairly high energies, being superimposed to the signal of all elements present.

Finally, one further effect was considered in order to obtain the almost perfect simulation seen in the low energy

region, down to the low level discrimination of the MCA. Usually the beam is followed with its average energy; when this average energy reaches zero energy, the calculation is stopped, even if about half of the beam ions still has positive energies. This leads to simulated signals always smaller than the data. We developed recently an algorithm that follows the beam energy distribution, not until its maximum is at zero, but until all ions have been stopped [12]. Furthermore, NDF considers not channel zero, but energy zero. This implies, given that the energy calibration often has a positive offset, to calculate the yield for virtual negative channels, that due to the energy spread still lead to counts in real channels. This is essential to reproduce the yield at very low energies.

Buried resonances, i.e. resonances that occur deep in the sample, when the energy spread of the incoming beam is of the order of magnitude of the resonance width, are also not trivial to simulate correctly [13,14]. Usually, the non-Rutherford scattering cross section is taken for the average beam energy before scattering. This can lead to large errors if the cross section changes significantly within the incoming beam energy distribution. Not only the shape of the
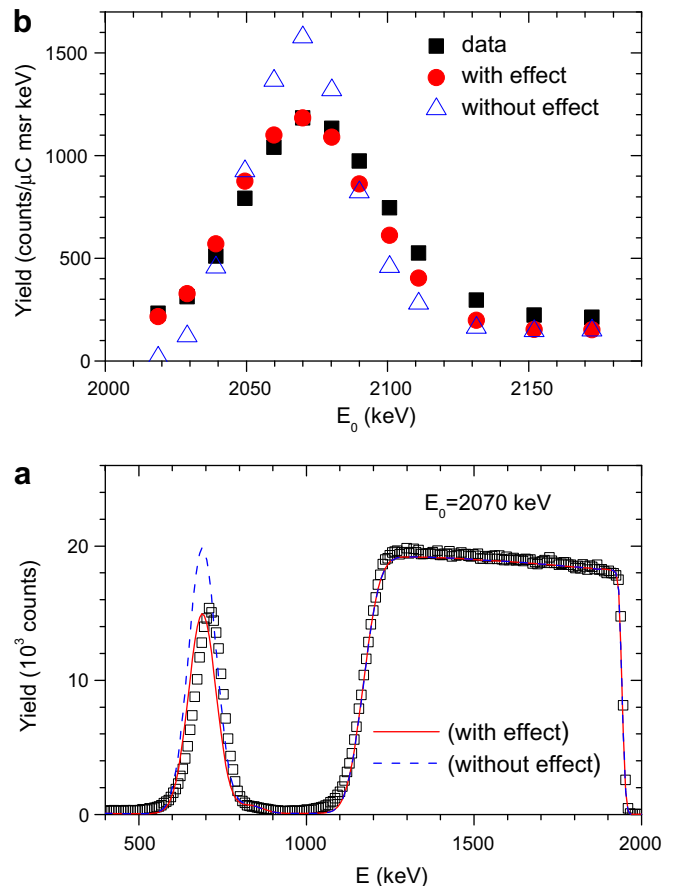

Fig. 2. (a) RBS spectrum of a Mylar 1 μm/Ni 4.2 μm sample, collected at $E_0 = 2070$ keV. (b) Integrated C yield as a function of beam energy. The data and calculated values with and without the resonance effect are shown.

resonance will be different, but the total yield from a thin film will also change. We developed recently an algorithm that correctly calculates both the width and size of resonances [15].

We measured a Mylar 1 μm/Ni 4.2 μm sample. The proton beam first crossed the Ni film leading to a high energy spread at the Mylar. We then collected many RBS spectra for different initial beam energy. The spectrum collected at $E_0 = 2070$ keV is shown in Fig. 2(a). This is designed to reach the centre of the Mylar film with an average energy close to the 1734 keV C resonance, and the C yield is at the maximum; without the resonance effect, the calculated yield is too large by around 35%. In Fig. 2(b) we show the experimental C resonance yield as a function of initial beam energy, together with the calculated yield calculated with and without the resonance effect, demonstrating the accuracy of the improved calculation.

3. Advanced algorithms

One of the important points in NDF is that it supports PIXE, being the sole code for general analysis of IBA data [13,14] that fully integrates PIXE with RBS, ERDA, and NRA [16,17]. Any number of spectra collected from the same sample, taken with any of these techniques in any experimental condition, can be analysed simultaneously with the same depth profile as fit parameter [18]. All complementary information present in each spectrum is thus used to generate one single solution, consistent with all data. Incidentally, this makes differential PIXE trivial to do [17].

The depth profile is represented as usual by finite layers with constant concentration. Function profiles are also supported. However, the logical fitting elements do not need to be individual elements. The user can define molecules, with stoichiometry pre-defined or to be fitted. Complex molecules composed of sub-molecules are also allowed (see below). This allows the user, on the one hand, to introduce known elemental chemistry. For instance, if SiO_2, instead of Si and O separately, is given as logical element, only physically correct solutions will be found. On the other hand, with molecules the signal of different elements becomes correlated, which is particularly important when light and heavy elements co-exist. For instance, the data shown in Fig. 1 were analysed with $Ti_xAl_yN_z$ as logical element, where x, y and z were the fitting parameters. The molecular stoichiometry is thus kept the same in all layers. As the Ti and Al multilayer oscillations are clearly observed, this means that the N concentration can also be derived.

We show in Fig. 3(a) the EBS spectrum collected with a 2.582 MeV $^1H^+$ beam from a carbon nanotube sample boiled for 2 h in 18 MΩ water [19] and analysed on a transmission polypropylene foil with RBS, EBS, and PIXE. The details of the sample preparation and IBA analysis are given elsewhere [19,20]. The presence of Pt, Re, Rh, Fe, Cu and Cl contaminants was detected by PIXE at concen-
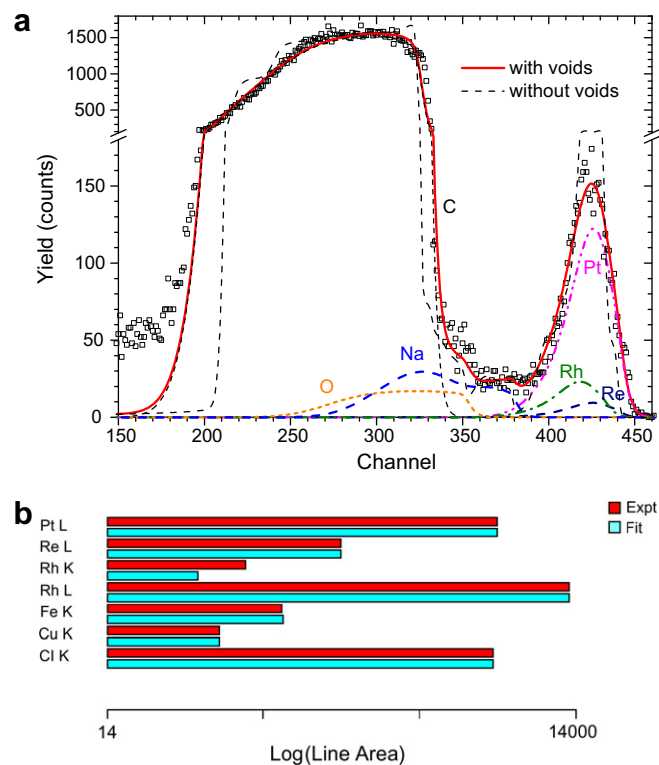

Fig. 3. (a) 2.582 MeV $^1H^+$ EBS spectrum beam from a carbon nanotube sample boiled for 2 h in 18MΩ water and analysed on a transmission polypropylene foil. (b) PIXE results.

trations between 0.002 and 0.8 at.%. Na and O are visible in the EBS data.

The sample has 10 elements, leading to superimposed partial spectra with very small signals. Several of the elements have yields below 2 counts per channel This spectrum is virtually impossible to analyse by traditional means. However, using complex molecules as logical elements together with the PIXE information, meaningful analysis can be made.

We first defined one molecule, CH_2, for the substrate. A second molecule includes the heavier metals Pt, Re, and Rh which are clearly visible in the data with changing concentration. The elemental ratio of this molecule was fixed by the PIXE data. As mentioned above, the yield of the other contaminants is too small to be detected. So, in a first step we kept the Fe:Cu:Na:Cl ratio as measured with PIXE. At the same time we linked the small O yield to the C by defining a $C_{1-x}O_x$ logical unit with $x \approx 0.01$ to be fitted. We then linked the (Fe:Cu:Na:Cl) to the $C_{1-x}O_x$, by defining a composite molecule: $(C_{1-x}O_x)_{1-y}$:(Fe:Cu:Na:Cl)$_y$, where the $y \approx 0.0025$ is also a fit parameter. It is this composite molecule, as a whole, that is treated as a logical unit in the analyses process: the molecular concentration in each layer is a fit parameter; the individual C, O, Fe, etc. concentrations are not.

It is also required to take into account the fact that most of this sample is actually empty space. NDF can include the effect of voids and inclusions [21,8]. In this case we

considered a high fraction of voids, slightly higher at the surface to simulate the gross surface roughness. A simulation without these effects is also shown in Fig. 3.

NDF uses as fitting algorithm simulated annealing (SA) [22], complemented by a local search. SA is fully automatic, does not require an initial guess, and so leads to high quality solutions with minimum user intervention [23]. Besides the depth profile (given as elements or molecules, or any combination of those), other parameters that can be fitted are the experimental conditions (beam energy, scattering and incidence angles, charge), and roughness parameters if present.

Given that RBS and IBA in general are fully quantitative techniques, with quantifiable associated uncertainties, error bars on the depth profiles derived should be possible to calculate, but are almost never presented. We thus developed a Bayesian inference (BI) algorithm with the Markov chain Monte Carlo technique [24] to systematically calculate limits of confidence in the results obtained. This is based on generating randomly a sequence of depth profiles that all lead to a good fit to the data within errors. For the data shown in Fig. 1, we derive $x = 19.2 \pm 0.9$, $y = 31.1 \pm 0.9$ and $z = 49.6 \pm 1.7$, which is very close to the 2:3:5 expected stoichiometry.

We have also applied BI to the determination of stopping powers [25] and scattering cross sections [26] from simple RBS spectra. The method is based on collecting a series of spectra at different beam energies, and analysing them all simultaneously, with the continuous stopping power or cross section curve treated as fit parameters. For ^{4}He in Si, results equivalent within the experimental uncertainty to SRIM03 version 2006.02 [27] and Konac et al. [28] were obtained [25].

One of the problems in BI is to find a transition function that leads from one state (depth profile and other parameters) to the next one in a random, but efficient, way. If the perturbation introduced is too large, very few transitions are accepted. If it is too small, all transitions are accepted but it takes a very long time to explore the whole parameter space. We introduced in NDF the following method: Let Y_k and I_k be the calculated and measured yield in channel k, respectively, and σ_k be the error in I_k. Their difference is $\Delta Y_k = I_k - Y_k$. The experimental error in channel k is σ_k. $Y_k = f(r)$ is some unspecified function of a parameter to be determined r.

We want to know the influence of a change δr of the parameter r in the χ^2, which can be taken as the likelihood. The change in Y_k will be

$$\delta Y_k = \delta f / \delta r \, \delta r = f' \delta r, \tag{1}$$

where f' is calculated separately for each channel k. The new χ^2 will be

$$\chi^2 = \sum_k (\Delta Y_k - f' \delta r)^2 / \delta_k^2. \tag{2}$$

The change in r that leads to the smallest χ^2 is

$$\delta r = \sum_k f' \Delta Y_k / \sigma_k^2 / \sum_k f'^2 / \sigma_k^2 \tag{3}$$

The sum is made over all channels affected by the parameter r. This is done parameter by parameter, for instance for concentrations, this is done layer by layer, element by element. This leads to an efficient optimisation procedure, which is not what is required for BI. Instead, we calculate the error σ_r on δr

$$\sigma_r = \sqrt{S / (S S_{XX} - S_{XX}^2)} \tag{4}$$

with

$$S = \sum_k 1/\sigma_k^2, \quad S_X = \sum_k f'/\sigma_k^2, \quad \text{and} \quad S_{XX} = \sum_k f'^2/\sigma_k^2 \tag{5}$$

We then make random perturbations of parameter r; the perturbations follow a Gaussian distribution with standard deviation σ_r, which ensures that the new calculated spectrum changes in a way commensurate to the error in each channel. That is, the transitions are on average exactly as large as the experimental error allows them to be, which leads to an acceptance ratio of proposed transitions close to 100%.

The crucial point is to calculate f'. Beam fluence has a linear influence on the spectrum leading to a trivial $f'(r)$. The concentration of a given element in a given layer leads, in first approximation, also to a linear change of the corresponding yield, and f' is also trivial. For the other cases, we calculate f' numerically.

4. Summary

We presented recent developments in the IBA DataFurnace (NDF) code for analysis of RBS, ERDA, NRA, and PIXE data. We utilised some difficult examples from real life experiments to show how it is essential to include advanced physics in the analysis of complex data, and also how advanced algorithms can assist the user in retrieving efficiently all the information present in the data.

References

[1] C. Jeynes, N.P. Barradas, P.K. Marriott, G. Boudreault, M. Jenkin, E. Wendler, R.P. Webb, J. Phys. D: Appl. Phys. 36 (2003) R97.
[2] C.J. Tavares, L. Rebouta, E. Alves, N.P. Barradas, J. Pacaud, J.P. Riviére, Nucl. Instr. and Meth. B 188 (2002) 90.
[3] N.P. Barradas, A. Fonseca, N. Franco, E. Alves, Nucl. Instr. and Meth. B 241 (2005) 316.
[4] E. Szilágyi, Nucl. Instr. and Meth. B 161–163 (2000) 37.
[5] G. Amsel, G. Battistig, A. L'Hoir, Nucl. Instr. and Meth. B 201 (2003) 325.
[6] N.P. Barradas, J. Phys. D: Appl. Phys. 34 (2001) 2109.
[7] N.P. Barradas, E. Alves, S. Pereira, V.V. Shvartsman, A.L. Kholkin, E. Pereira, K.P. O'Donnell, C. Liu, C.J. Deatcher, I.M. Watson, M. Mayer, Nucl. Instr. and Meth. B 217 (2004) 479.
[8] N.P. Barradas, Nucl. Instr. and Meth. B 261 (2007) 435.
[9] N.P. Barradas, M. Reis, X-Ray Spectrom. 35 (2006) 232.
[10] L. Wielopolski, R.P. Gardner, Nucl. Instr. and Meth. 133 (1976) 303.
[11] N.P. Barradas, Nucl. Instr. and Meth. B 225 (2004) 318.
[12] N.P. Barradas, Nucl. Instr. and Meth. B 261 (2007) 418.

[13] E. Rauhala, N.P. Barradas, S. Fazinić, M. Mayer, E. Szilágyi, M. Thompson, Nucl. Instr. and Meth. B 244 (2006) 436.

[14] N.P. Barradas, K. Arstila, G. Battistig, M. Bianconi, N. Dytlewski, C. Jeynes, E. Kótai, G. Lulli, M. Mayer, E. Rauhala, E. Szilágyi, M. Thompson, Nucl. Instr. and Meth. B 262 (2007) 282.

[15] N.P. Barradas, E. Alves, C. Jeynes, M. Tosaki, Nucl. Instr. and Meth. B 247 (2006) 381.

[16] Carlos Pascual-Izarra, N.P. Barradas, Miguel A. Reis, Nucl. Instr. and Meth. B 249 (2006) 820.

[17] Carlos Pascual-Izarra, Miguel A. Reis, N.P. Barradas, Nucl. Instr. and Meth. B 249 (2006) 780.

[18] N.P. Barradas, C. Jeynes, R.P. Webb, U. Kreissig, R. Grötzschel, Nucl. Instr. and Meth. B 149 (1999) 233.

[19] J.C.G. Jeynes, Nucl. Instr. and Meth. B, these proceedings.

[20] R. Schönfelder, M.H. Rümmeli, W. Gruner, M. Löffler, J. Acker, V. Hoffmann, T. Gemming, B. Büchner, T. Pichler, Nanotechnology 18 (2007) 375601.

[21] J.P. Stoquert, T. Szörenyi, Phys. Rev. B 66 (2002) 144108.

[22] Emile Aarts, Jan Korst, Simulated Annealing and Boltzmann Machines: A Stochastic Approach to Combinatorial Optimization and Neural Computing, Wiley, Chichester, 1989.

[23] N.P. Barradas, C. Jeynes, M.A. Harry, Nucl. Instr. and Meth. B 136–138 (1998) 1163.

[24] N.P. Barradas, C. Jeynes, M. Jenkin, P.K. Marriott, Thin Solid Films 343–344 (1999) 31.

[25] N.P. Barradas, C. Jeynes, R.P. Webb, E. Wendler, Nucl. Instr. and Meth. B 194 (2002) 15.

[26] N.P. Barradas, A.R. Ramos Wahl, E. Alves, Nucl. Instr. and Meth. B, these proceedings.

[27] www.SRIM.org; J.F. Ziegler, Nucl. Instr. and Meth. B 219–220 (2004) 1027.

[28] G. Konac, S. Kalbitzer, C. Klatt, D. Niemann, R. Stoll, Nucl. Instr. and Meth. B 136–138 (1998) 159.